



## Metastatic state of parent cells influences the uptake and functionality of prostate cancer cell-derived extracellular vesicles

Elisa Lázaro-Ibáñez , Maarit Neuvonen , Maarit Takatalo , Uma Thanigai Arasu, Cristian Capasso, Vincenzo Cerullo , Johng S. Rhim, Kirsi Rilla , Marjo Yliperttula & Pia R.-M. Siljander

To cite this article: Elisa Lázaro-Ibáñez , Maarit Neuvonen , Maarit Takatalo , Uma Thanigai Arasu, Cristian Capasso, Vincenzo Cerullo , Johng S. Rhim, Kirsi Rilla , Marjo Yliperttula & Pia R.-M. Siljander (2017) Metastatic state of parent cells influences the uptake and functionality of prostate cancer cell-derived extracellular vesicles, Journal of Extracellular Vesicles, 6:1, 1354645, DOI: [10.1080/20013078.2017.1354645](https://doi.org/10.1080/20013078.2017.1354645)

To link to this article: <http://dx.doi.org/10.1080/20013078.2017.1354645>



© 2017 The Author(s). Published by Informa UK Limited, trading as Taylor & Francis Group.



[View supplementary material](#)



Published online: 10 Aug 2017.



[Submit your article to this journal](#)



Article views: 76



[View related articles](#)




[View Crossmark data](#)

RESEARCH ARTICLE



## Metastatic state of parent cells influences the uptake and functionality of prostate cancer cell-derived extracellular vesicles

Elisa Lázaro-Ibáñez <sup>a</sup>, Maarit Neuvonen <sup>a,b</sup>, Maarit Takatalo <sup>a,b</sup>, Uma Thanigai Arasu<sup>c</sup>, Cristian Capasso<sup>d</sup>, Vincenzo Cerullo <sup>d</sup>, Johng S. Rhim<sup>e</sup>, Kirsi Rilla <sup>c</sup>, Marjo Yliperttula<sup>a</sup> and Pia R.-M. Siljander <sup>a,b</sup>

<sup>a</sup>Division of Pharmaceutical Biosciences, Centre for Drug Research, Faculty of Pharmacy, University of Helsinki, Helsinki, Finland; <sup>b</sup>Division of Biochemistry and Biotechnology, Department of Biosciences, University of Helsinki, Helsinki, Finland; <sup>c</sup>Faculty of Health Sciences, School of Medicine, Institute of Biomedicine, University of Eastern Finland, Kuopio, Finland; <sup>d</sup>Laboratory of Immunovirotherapy, Division of Pharmaceutical Biosciences and Centre for Drug Research, University of Helsinki, Helsinki, Finland; <sup>e</sup>Center for Prostate Disease Research, Department of Surgery, Uniformed Services University of Health Sciences, Bethesda, MD, USA

### ABSTRACT

Extracellular vesicles (EVs), including microvesicles and exosomes, mediate intercellular signalling which has a profound role in cancer progression and in the development of metastasis. Internalisation of EVs can prompt functional changes in the recipient cells, the nature of which depends on the molecular composition and the cargo of the EVs. We hypothesised that the metastatic stage of cancerous parent cells would determine the uptake efficacy and the subsequent functional effects of the respective cancer cell-derived EVs. To address this question, we compared the internalisation of EVs derived from two metastatic site-derived prostate cancer cell lines (PC-3 and LNCaP), human telomerase reverse transcriptase immortalised primary malignant prostate epithelial cells (RC92a/hTERT), and a benign epithelial prostate cell line (PNT2). EVs isolated from the metastatic site-derived PC-3 and LNCaP cells were more efficiently internalised by the PC-3 and PNT2 cells compared to the EVs from the primary malignant RC92a/hTERT cells or the benign PNT2 cells, as determined by high content microscopy, confocal microscopy, and flow cytometry. EV uptake was also influenced by the phase of the cell cycle, so that an increased EV-derived fluorescence signal was observed in the cells at the G<sub>2</sub>/M phase compared to the G<sub>0</sub>/G<sub>1</sub> or S phases. Finally, differences were also observed in the functions of the recipient cells based on the EV source. Proliferation of PNT2 cells and to a lesser extent also PC-3 cells was enhanced particularly by the EVs from the metastatic-site-derived prostate cancer cells in comparison to the EVs from the benign cells or primary cancer cells, whereas migration of PC-3 cells was enhanced by all cancerous EVs.

### ARTICLE HISTORY

Received 8 March 2017  
Accepted 4 July 2017

### RESPONSIBLE EDITOR

Takahiro Ochiya, National Cancer Center, Japan




### KEYWORDS

Extracellular vesicles; uptake; prostate cancer; cell cycle; cell proliferation; cell migration


## Introduction

Exchange of molecular information during intercellular communication is essential for cell survival and function. In addition to soluble factors, this communication is mediated by cell-derived extracellular vesicles (EVs), which are internalised by recipient cells during normal physiological, but also during pathological processes [1,2]. EVs, most likely released by all cell types, are a heterogeneous population of vesicles, comprising e.g. microvesicles (MVs) (~100–1000 nm diameter) and exosomes (EXOs) (~50–150 nm diameter) [3]. The diversity of the vesicles within the EV pool from a given cell is dependent on the state of the parent cell and the conditions relating to e.g. cell growth, activation, and cellular microenvironment [3,4].

EVs are gaining increasing interest due to their ability to impact cellular reprogramming of the recipient cells by the delivery of functional molecules, from nucleic acids to proteins, lipids, and metabolites [5–9]. The delivery of the EV cargo has been shown to contribute to the transformation of the recipient cell phenotype during tumour development and to the metastatic niche formation [10–13], and cancer-derived EV adhesion molecules have been shown to predict the site of metastasis [14]. Also regarding prostate cancer (PCa), there is increasing evidence supporting an active role of EVs in PCa progression by stimulating e.g. malignant cellular transformation [15,16], the exchange of molecular information with neighbouring cells [9,17,18], fibroblast activation [19], and osteoblast differentiation during metastasis [20]. Examples of EV-borne PCa molecular secretome include

**CONTACT** Pia R.-M. Siljander  [pia.siljander@helsinki.fi](mailto:pia.siljander@helsinki.fi); Elisa Lázaro-Ibáñez  [elisa.lazaroibanez@astrazeneca.com](mailto:elisa.lazaroibanez@astrazeneca.com)  Division of Pharmaceutical Biosciences, Centre for Drug Research, Faculty of Pharmacy, University of Helsinki, Helsinki 00014, Finland

Elisa Lázaro-Ibáñez is currently a full-time employee of AstraZeneca AB R&D.

 Supplemental data for this article can be accessed [here](#).

© 2017 The Author(s). Published by Informa UK Limited, trading as Taylor & Francis Group.

This is an Open Access article distributed under the terms of the Creative Commons Attribution-NonCommercial License (<http://creativecommons.org/licenses/by-nc/4.0/>), which permits unrestricted non-commercial use, distribution, and reproduction in any medium, provided the original work is properly cited.

the abundance of certain microRNAs [21], proteins [22,23], and gDNA harbouring tumour-related mutations [24]. Recently, we showed that metastatic PCa-derived EVs carried distinctly enriched mRNA signatures different from each other and from the benign prostate epithelial EVs, and that these signatures could be associated with the stage of tumour progression [25]. Specific mRNA cargo of PCa EVs has been associated with transcriptomic changes in PCa cells [26] and the predictability of disease aggressiveness [27]. However, to date, no study has systematically addressed the uptake and functional properties of EVs released from prostate cells with varying degrees of malignancy in the same experimental settings.

For the present study, we isolated and compared EVs from four prostate cell lines: metastatic site-derived LNCaP and PC-3 cells, the human immortalised primary malignant prostate epithelial RC92a/hTERT cells, and the benign prostate epithelial PNT2 cells. We show that the efficiency of the EV uptake depended on the metastatic status of the parent cells as well as on the cell cycle phase of the recipient cells. Finally, internalisation of the metastatic cell-derived EVs was shown to efficiently promote proliferation and migration in recipient cells.

## Material and methods

### Cell lines and culture conditions

PCa metastatic site-derived LNCaP and PC-3 cells (ATCC, Manassas, VA, USA), human immortalised benign prostate epithelial PNT2 cells (ECACC, Salisbury, UK), and human immortalised primary malignant prostate epithelial RC92a/hTERT cells [28] were used in the study. PNT2 and RC92a/hTERT cells were grown in serum-free keratinocyte medium supplemented with bovine pituitary extract and human recombinant epidermal growth factor. LNCaP and PC-3 cells were grown in RPMI 1640 and DMEM/F12 media respectively, supplemented with 10% EV-depleted foetal bovine serum. All media were supplemented with 100 IU ml<sup>-1</sup> of penicillin and 100 µg ml<sup>-1</sup> streptomycin and filtered through 0.22 µm filter (Merck Millipore, Merck KGaA, Darmstadt, Germany) before addition to cells. The EV-depleted serum was produced by ultracentrifugation at 110,000 × g<sub>avg</sub> for 16 h using a 50.2 Ti rotor (Beckman Coulter, Brea, CA, USA), followed by filtration through a 0.22 µm filter. Cells were grown at 37°C and 5% of CO<sub>2</sub> atmosphere and maintained in their own media during experiments. All reagents were obtained from Thermo Fisher Scientific (Thermo Fisher, Waltham, MA, USA). PNT2 and PC-3 cell growth was analysed as index doubling times using RTCA iCELLigence machine (ACEA Biosciences, San Diego, CA, USA). PC-3 and PNT2 cells

were divided in their respective mediums on E L8 PET-plates in twofold dilution series (40,000 to 5000 cells/well) in duplicates and allowed to attach for 30 min at RT before the plates were transferred to the iCELLigence machine and the program for proliferation was used. The optimal growth density was used for doubling time analysis within 48 h after seeding.

### EV isolation and labelling

When cells reached 80% confluence, which was achieved in three days by PC-3 cells and in four days by LNCaP, RC92a/hTERT and PNT2 cells, the complete cell-conditioned medium was collected and centrifuged at 1000 × g for 10 min and 2500 × g for 25 min to remove cell debris and apoptotic bodies. The supernatant was centrifuged at 20,000 × g for 60 min using a SLA 1500 rotor (Sorvall) to obtain the 20K MV-enriched fraction. The resulting supernatant was ultracentrifuged at 110,000 × g<sub>avg</sub> for 2 h using an Optima-LE 80K ultracentrifuge, 50.2 Ti rotor, k-factor 143.3 (Beckman Coulter) to obtain the 110K EXO-enriched fractions. The pellets were resuspended in DPBS (Thermo Fisher Scientific) and stored at -80°C. For controls, the completed cell media that has not been in contact with cells was subjected to EV isolation. Particle counts close to background levels of buffers were identified, and were at least 100-fold lower compared to the MV and EXO samples.

EVs were labelled with fluorescent lipophilic tracers: DiIC<sub>18</sub>(5)-DS (DiIC<sub>18</sub>) (1–2 µg ml<sup>-1</sup>) or SP-DiOC<sub>18</sub>(3) (DiOC<sub>18</sub>) (2 µg ml<sup>-1</sup>) (Molecular Probes, Thermo Fisher Scientific) for 20 min at 37°C, and the unbound dye was removed by ultracentrifugation at 110,000 × g<sub>avg</sub> for 1 h using Optima MAX-XP ultracentrifuge with TLA-55 rotor, k-factor 81.3 (Beckman Coulter). Efficacy of labelling was verified with flow cytometry using Apogee A50 micro (Apogee, Apogee Flow Systems, Hertfordshire, UK). The diluted dye alone subjected to the same ultracentrifugation protocol as EVs was used as a mock control. The samples were measured for 120 s with optimal settings. Then SDS was added to a final concentration of 0.15% to dissolve EVs and the samples were re-measured. The change in the fluorescent intensity of DiOC<sub>18</sub>-EV samples with and without SDS was analysed to demonstrate the specificity of the labelling.

### Transmission electron microscopy

EV samples were visualised with a transmission electron microscope (FEI Tecnai Spirit G2, FEI Company, Eindhoven, The Netherlands) at 80 kV and a digital camera (Soft Imaging System GmbH, Münster,

Germany) as previously reported [24]. Briefly, EV samples were incubated on glow discharged 200 mesh formvar copper grids for 2 min at 4°C. Next, the grids were washed with distilled water, negatively stained with 2% aqueous uranyl acetate (Sigma-Aldrich, Merck KGaA), washed again, and dried in darkness.

### **Nanoparticle tracking analysis**

A nanoparticle tracking analyser (NTA) (Malvern Instruments Ltd, Malvern, UK) with a LM14 view unit, blue laser (405 nm, 70mW) and a sCMOS camera (Hamamatsu Photonics, Hamamatsu, Japan) was used to measure the size distribution and concentration of EVs. Triplicate measurements under constant equipment settings were conducted as follows: camera level 14, auto-settings off, reproducibility and polydispersity high, acquisition time 90 s, < 100 particles per image, screen gain 10, and threshold 10. Data analysis was performed with the NTA 2.3 software (NanoSight, Amesbury, UK).

### **Protein quantification and Western blotting**

Samples were lysed with RIPA buffer (Pierce, Thermo Scientific) supplemented with a protease inhibitor mixture (Sigma-Aldrich). Protein concentration was determined with microBCA protein assay following the manufacturer's recommendations (Pierce, Thermo Scientific). For SDS-PAGE, samples were prepared in Laemmli buffer (Bio-Rad, Hercules, CA, USA) under non-reducing conditions, and 25 µg of samples were loaded in 10–12% Mini-PROTEAN TGX™ gels (Bio-Rad) and transferred onto Protran nitrocellulose membrane. Membranes were blocked with 5% blotting-grade non-fat dry milk (Bio-Rad) in Tris-buffered saline (TBS) for 1 h at room temperature (RT). Primary antibodies were diluted in 2.5% milk-TBS: mouse monoclonal anti-CD9 (ALB 6, 1:200) and anti-GAPDH (7B, 1:500) from Santa Cruz Biotechnology (Dallas, TX, USA), anti-CD63 (H5C6, 1:200) and anti-HSP70 (7, 1:2000) from BD Pharmingen (BD Biosciences, San Jose, CA, USA), were used for Western blotting. Membranes were washed three times with TBS-0.1% Tween 20 (TBST), and incubated for 45 min at RT with the goat anti-mouse IgG-HRP secondary antibody (Santa Cruz Biotechnology) diluted in 2.5% milk-TBST. Membranes were washed, incubated with Luminata Crescendo Western HRP Substrate (Merck Millipore, Merck KGaA, Darmstadt, Germany), and visualised on Amersham Hyperfilm ECL (GE Healthcare Ltd, Chicago, IL, USA).

### **EV uptake analysis by IN Cell Analyser 1000 high content microscopy**

Cells were seeded in black clear bottom 96-well plates at a density of 4000 cells/well, except PC-3 3000 cells/well, and labelled with CellBrite Green Cytoplasmic Dye (Biotium, Fremont, CA, USA), according to the manufacturer's instructions. Next day, media supplemented with  $10^9$  particles  $\text{ml}^{-1}$  of DiIC<sub>18</sub>-20K MVs or 110K EXOs was added. Each cell line was incubated with 20K MVs and 110K EXOs from the four cell types. Cells were stained with Hoechst, and analysed using an IN Cell Analyser 1000 (GE Healthcare, Life Sciences) with a CCD camera and a 20×/0.45 NA objective. The 51,008 polychromic mirror set was used together with the filter combinations: (405/20 nm excitation, 535/50 nm emission) for nuclei, (475/20 nm excitation, 535/50 nm emission) for cytoplasm, and (620/60 nm excitation, 700/75 nm emission) for DiIC<sub>18</sub>-EVs. Analysis was performed using the Developer Toolbox 1.7 software (GE Healthcare) and parameters were kept constant between different samples. The percentage of cells with DiOC<sub>18</sub>-EV was quantified using segmentation algorithms selecting EVs as a region of interest (ROI) and normalised to the total number of cells.

### **EV uptake and cell cycle analysis by flow cytometry**

PC-3 and PNT2 cells were seeded in six-well plates (Corning Costar, Sigma Aldrich) at 300,000 cells/well and incubated with different EVs. For cell cycle experiments, PC-3 cells were incubated with LNCaP or PC-3 EVs. Once 80% confluent,  $10^9$  particles  $\text{ml}^{-1}$  of DiIC<sub>18</sub>-EVs (for uptake) or DiOC<sub>18</sub>-EVs (for cell cycle) experiments were added to the cultures. Following incubations at different time points, cells were washed twice with DPBS, harvested, fixed overnight with cold 99% ethanol, and stored at –20°C. Following ethanol removal and rehydration, cell cycle samples were stained with 3 µM propidium iodide (Molecular Probes, Thermo Fisher Scientific) in 4% FBS-DPBS for 15 min at RT. All samples were analysed with a Gallios flow cytometer (Beckman Coulter) and data were analysed with FlowJo 10.0 software (FlowJo LLC, Ashland, Oregon, USA). At least 20,000 events/sample were recorded. Unstained cells with and without EVs were used as negative controls to gate the positive populations. Normalised geometric mean fluorescent intensity (gMFI) of cells ± SEM was presented for each time point.

### **Immunostaining and confocal microscopy**

Cells were plated in chamber slides (Ibidi GmbH, Martinsried, Germany) and treated with  $10^9$  particles  $\text{ml}^{-1}$  of DiIC<sub>18</sub>-EVs. After 16 h or 24 h of incubation, the

cells were fixed with 4% paraformaldehyde, permeabilised with 0.1% Triton X-100 in 1% BSA-PBS and blocked with 1% BSA-PBS. Samples were stained at 4°C overnight with anti-CD44 (1:200, gift from Dr Jalkanen, Turku, Finland), anti-Lamp1 (H4A3, 1:100, IOWA University, Developmental Studies, USA), polyclonal anti-GM130 (1:100) or anti-EEA1 (1:100) (Cell Signaling, Danvers, MA, USA). After washing, the cells were incubated for 1 h at RT with Texas red anti-mouse (1:100) or Texas red anti-rabbit (1:500), (Vector Laboratories, Peterborough, UK). The nuclei were stained with DAPI (1  $\mu\text{g ml}^{-1}$ , Sigma-Aldrich). Confocal images were obtained with Zeiss Axio Observer with Zeiss LSM 800 confocal module (Carl Zeiss Microimaging GmbH, Jena, Germany) using sequential scanning. Co-localisation analyses were conducted using Imaris 7.7.2 software (Bitplane Inc., Belfast, United Kingdom), selecting DiIC<sub>18</sub>-EVs channel as ROI. Thresholds were automatically adjusted by the software within the ROI. The percentage of ROI material of DiIC<sub>18</sub> co-localising with CD44, EEA1, Lamp-1 or GM130 markers was separately analysed from at least eight images containing multiple cells.

### CFSE proliferation assay

PC-3 and PNT2 cells were seeded in six-well plates and incubated with 5  $\mu\text{M}$  CellTrace carboxyfluorescein diacetate succinimidyl ester (CFSE) (Molecular Probes, Thermo Fisher Scientific, catalogue number C34554) for 20 min at 37°C. The residual CFSE was removed by three washes in 2% FBS-PBS and addition of fresh media to the cells. After 30 min, 10<sup>9</sup> particles ml<sup>-1</sup> of EVs were added to the wells. Cells were harvested in 2% FBS-PBS after 48 h or 72 h, labelled with 7-amino-actinomycin (7-AAD) (BD Pharmingen) to check cell viability, and immediately subjected to flow cytometry analysis. Fluorescence intensity was measured from 100,000 events with a FACS Verse flow cytometer (BD Biosciences, San Jose, CA, USA) and analysed with FlowJo. Cell proliferation results were expressed as fold increase compared with controls from three independent experiments  $\pm$  SEM.

### Migration assay

A radius 24-well assay fibronectin-coated kit (Cell Biolabs, San Diego, CA, USA) was used to determine the effect of EVs on cell migration according to manufacturer's instructions. Briefly, PC-3 cells were seeded at 200,000 cells/well. After gel removal, cells were incubated with 1 ml of EV-supplemented or normal media. Phase-contrast pre-migration images were captured with an inverted EVOS XL microscope (Thermo Fisher Scientific) at 10  $\times$  magnification. The gap closure was

monitored up to 9 h and data were analysed using ImageJ 1.49v software ([imagej.nih.gov/ij/](http://imagej.nih.gov/ij/)).

### Statistical analysis

Statistics were performed using GraphPad Prism 7.0 (GraphPad Software, San Diego, CA, USA). Unpaired Student's t-test, one-way or two-way ANOVA with Tukey's multiple comparisons test or Dunnett's multiple comparisons test were used.

## Results

### Characterisation of EVs derived from malignant and benign prostate cells

Cells used in this study were metastatic site-derived LNCaP and PC-3 PCa cells, RC92a/hTERT telomerase immortalised malignant primary prostate cells, and benign immortalised prostate epithelial PNT2 cells. The 20K MVs and 110K EXOs from these cells were isolated as enriched subpopulations using differential centrifugation and used as an entity or as separate populations. The amount of EVs released was in the range of 5–50  $\times 10^9$  particles ml<sup>-1</sup> per million cells for all the cell lines. Similar size distribution and morphology were observed for all of these EVs by transmission electron microscopy (Figure 1(a)). The majority of EVs in TEM were < 200 nm in diameter. In NTA, the hydrodynamic radius of 20K MVs and 110K EXOs overlapped and was larger for 20K MVs (mean size of 171.5  $\pm$  9.8 nm;  $n = 12$ ) than for 110K EXOs (mean size of 135.2  $\pm$  11.5 nm;  $n = 12$ ) combined for all the four cell lines. Characteristic EV transmembrane proteins CD9 and CD63 were detected from the 20K MVs and 110K EXOs with different ratios in comparison to their parent cells (Figure 1(b)). Similarly, the heat-shock protein 70 (HSP70) and glyceraldehyde-3-phosphate dehydrogenase (GAPDH) were differentially expressed in the EV subpopulations and their respective parent cell lysates. Due to the different cell media, the expression of these markers in EVs was not, however, directly comparable between the different cell sources.

The conditions for EV-labelling with fixable lipophilic dyes were optimised for uptake studies generating DiOC<sub>18</sub> labelled EVs that were clearly distinguished from the unlabelled EVs, as shown by a flow cytometer especially designed for small particles (Figure 1(c)). To verify that the fluorescent events were indeed EVs and not free dye in solution, the DiOC<sub>18</sub>-EVs were treated with a mild detergent, which shifted the fluorescent peak and its intensity by disrupting the EVs and releasing the bound dye (Figure 1(c)). Testing different EV

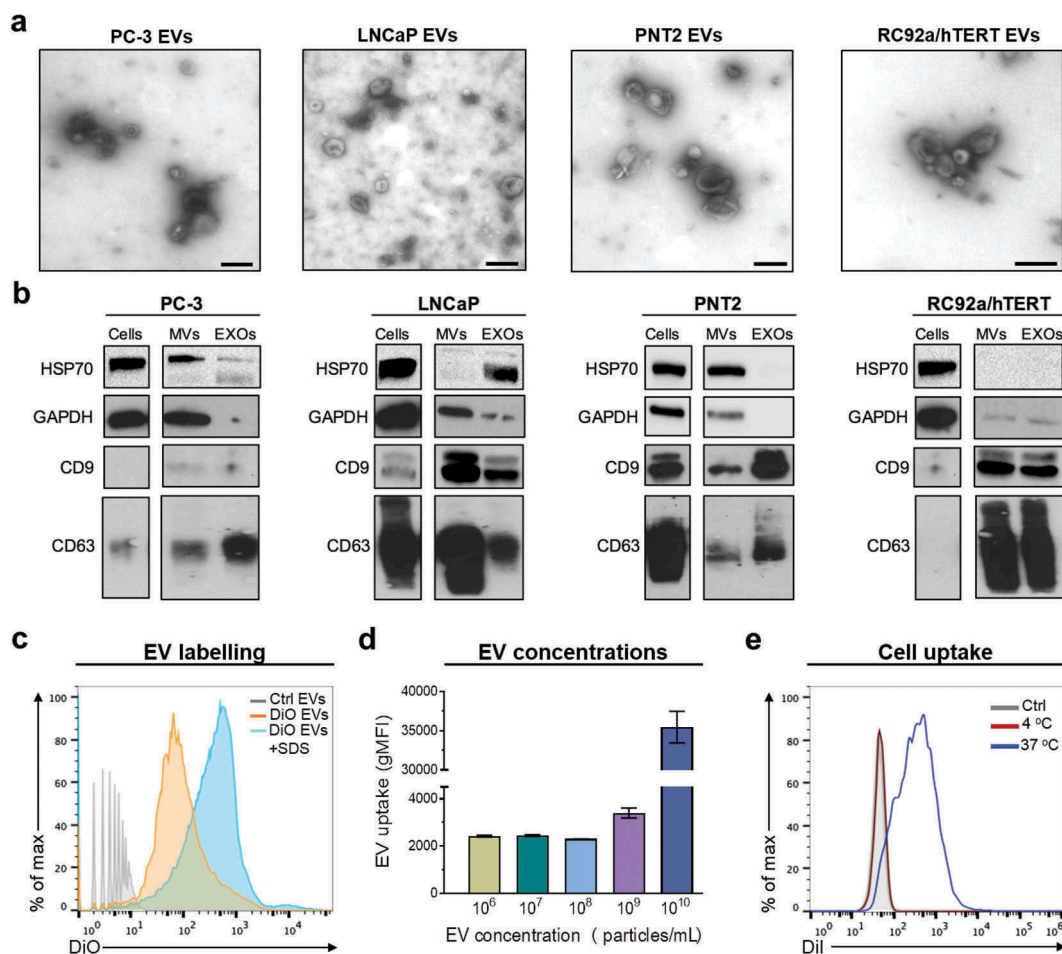


**Figure 1.** Characterisation and labelling of extracellular vesicles derived from different prostate cell lines. **(a)** Representative transmission electron micrographs of more than three independent preparations of EVs isolated from PC-3, LNCaP, PNT2, and RC92a/hTERT cell lines. Scale bars 200 nm. **(b)** Qualitative Western blot analysis of CD63, CD9, GAPDH, and HSP70 in the 20K microvesicles (MV), the 110K exosomes (EXOs) and cellular lysates. 25  $\mu$ g of total protein was loaded per lane. Images are representative of three independent experiments. **(c)** Representative histograms of the labelling efficacy of EVs using Apogee A50 micro flow cytometer. Unlabelled EVs (Ctrl), SP-DiOC<sub>18</sub>(3) labelled EVs (DiO EVs), and SP-DiOC<sub>18</sub>(3) labelled EVs after 0.15% SDS treatment (DiO EVs + SDS) ( $n = 2$ ). **(d)** Histograms of the uptake of different concentrations of SP-DiOC<sub>18</sub>(3) labelled EVs ( $10^6$ – $10^{10}$  particles  $\text{ml}^{-1}$ ) by PC-3 cells. Graphs represent the geometric mean fluorescence intensity (gMFI) of the cells with the different EV concentrations. Bars represent the mean  $\pm$  SEM of three independent experiments. **(e)** Representative histograms of three uptake experiments of DiIC<sub>18</sub>(5)-DS (DiI) labelled EVs by PC-3 cells after 3 h of incubation at 37°C and 4°C in comparison to the unstained EVs (Ctrl).

concentrations ( $10^6$ – $10^{10}$  particles  $\text{ml}^{-1}$ ) for the uptake experiments revealed that  $10^9$  particles  $\text{ml}^{-1}$  was the minimal EV concentration required to optimally detect EV uptake by flow cytometry (Figure 1(d)). This concentration was also in range with the EV concentrations secreted by these cells. Exposing cells to even higher EV concentrations further increased the uptake, suggesting that the intracellular EV load was not saturated at  $10^9$  particles  $\text{ml}^{-1}$ . To verify that the detected signal was from internalised EVs and not from EVs adhered to the cell surface, uptake at 4°C was analysed. The fluorescent signal in PC-3 cells incubated with DiIC<sub>18</sub>-EVs at 4°C was close to the background, as previously reported [29–31], in contrast to the signal observed at 37°C (Figure 1(e)).

### EVs derived from malignant and benign prostate cells exhibit different uptake kinetics

To investigate the time-dependent differences in the EV uptake, we used flow cytometry to quantitate the average intensity of DiIC<sub>18</sub>-labelled EVs/cell of the four different EV sources. Analysis was performed in PC-3 (Figure 2(a)) and PNT2 (Figure 2(b)) cells. A similar trend of EV uptake kinetics was observed in both cell types with no significant differences ( $p > 0.05$  two-way ANOVA) in the total EV uptake with the exception of more internalisation of PNT2 EVs into PNT2 cells than PC-3 cells at 12 h (Figure 2(a), 2(b)). Judging by the intensity/cell, the uptake of the PC-3 and LNCaP EVs by PC-3 cells was more efficient compared to the

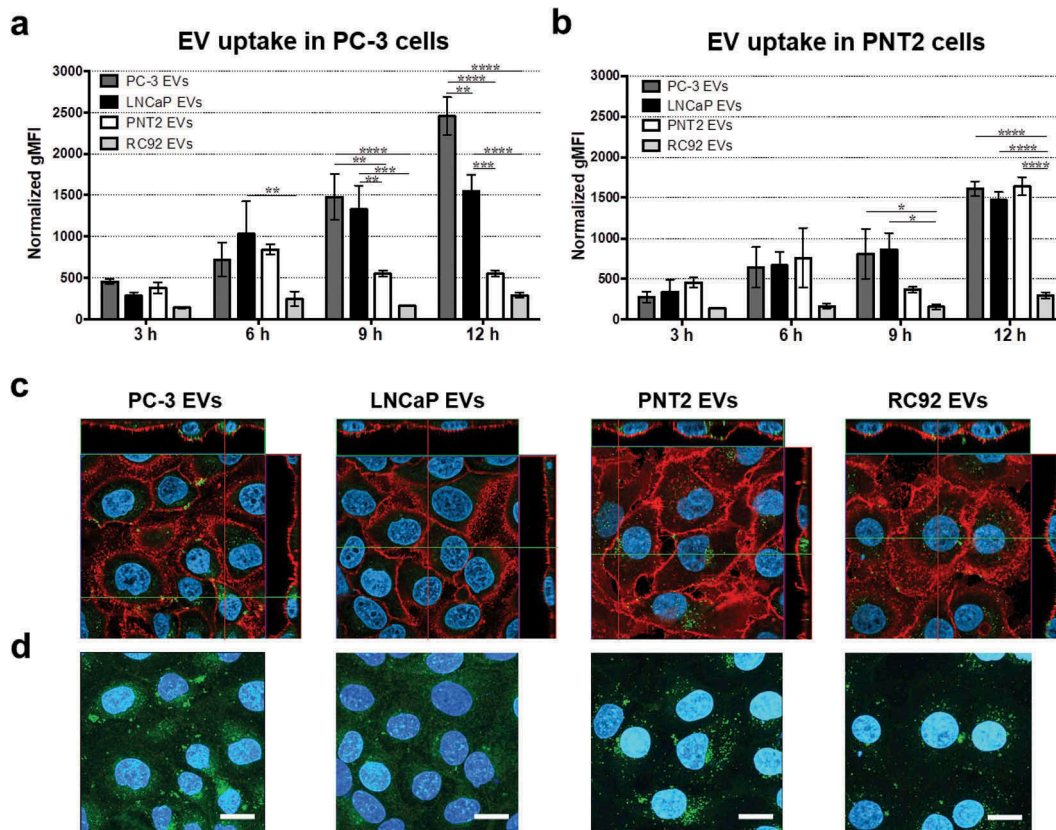


**Figure 2. Uptake of prostate cell-derived EVs analysed by flow cytometry and confocal microscopy.** Fluorescently labelled EVs ( $10^9$  particles  $\text{ml}^{-1}$ ) isolated from PC-3, LNCaP, PNT2 and RC92a/hTERT cells were incubated with (a) PC-3 and (b) PNT2 cells. Cells were analysed by flow cytometry and results were plotted as normalised geometric mean fluorescent intensity (gMFI) of EV fluorescence in cells. Bars represent mean  $\pm$  SEM of three independent experiments. \* $p < 0.05$ , \*\* $p < 0.01$ , \*\*\* $p < 0.001$ , \*\*\*\* $p < 0.0001$ , two-way ANOVA with Tukey's multiple comparisons test. (c) Representative confocal images of two different experiments per group depicting DiI<sub>18</sub>(5)-DS labelled EVs (pseudo-coloured green) incubated with PNT2 cells (plasma membrane marker CD44 pseudo-coloured red and nuclei blue) for 16 h. Middle images (optical sections), smaller images (vertical sections). (d) Maximum intensity projections created from stack of optical sections. Scale bars, 10  $\mu\text{m}$ .

uptake of PNT2 or RC92a/hTERT EVs at 9 and 12 h (Figure 2(a)). In PNT2 cells, the internalisation of PC-3 and LNCaP EVs was also significantly increased compared to RC92a/hTERT EVs at 9 and 12 h (Figure 2 (b)). The internalisation of PNT2 EVs by PNT2 cells did not significantly differ from the uptake of PC-3 and LNCaP EVs at 12 h, when judged by the label intensity/cell. Confocal microscopy analysis confirmed that the detected fluorescent signal was indeed from internalised EVs, and not from EVs bound to cell surface (PNT2 cells, Figure 2(c), 2(d)). Vertical sections generated by three dimensional analysis of confocal sections showed that the majority of the fluorescent EV signal was indeed observed inside the cells (Figure 2(c)).

To analyse the EV uptake by the number of cells internalising EVs, the percentage of EV-labelled positive cells was measured using automated high content microscopy. We also wanted to compare the uptake of the two EV subpopulations, 20K MVs and 110K EXOs. For this purpose, metastatic PC-3 (Figure 3(a)) and

benign PNT2 cells (Figure 3(b)) in exponential growth phase were incubated with PC-3, LNCaP, RC92a/hTERT, or PNT2-derived DiI<sub>18</sub>-labelled 20K MVs and 110K EXOs. Also in this assay, the uptake of metastatic site-derived EVs (PC-3, LNCaP) was clearly more efficient than the uptake of EVs from benign or primary cancer cells (PNT2, RC92a/hTERT). This phenomenon was detected both in the benign and metastatic recipient cells (PNT2 and PC-3). Faster and enhanced uptake of EVs from metastatic origin was obvious for both the 20K MV and 110K EXO populations. Thus, for the further analyses, we decided to investigate the differences between the EVs derived from metastatic or non-metastatic origin by using a pooled population of MVs and EXOs.

#### Cellular localisation of the EV-label after uptake

Next, we analysed the co-localisation of PNT2 and PC-3 DiI<sub>18</sub>-EVs with cellular organelles after 16 h of

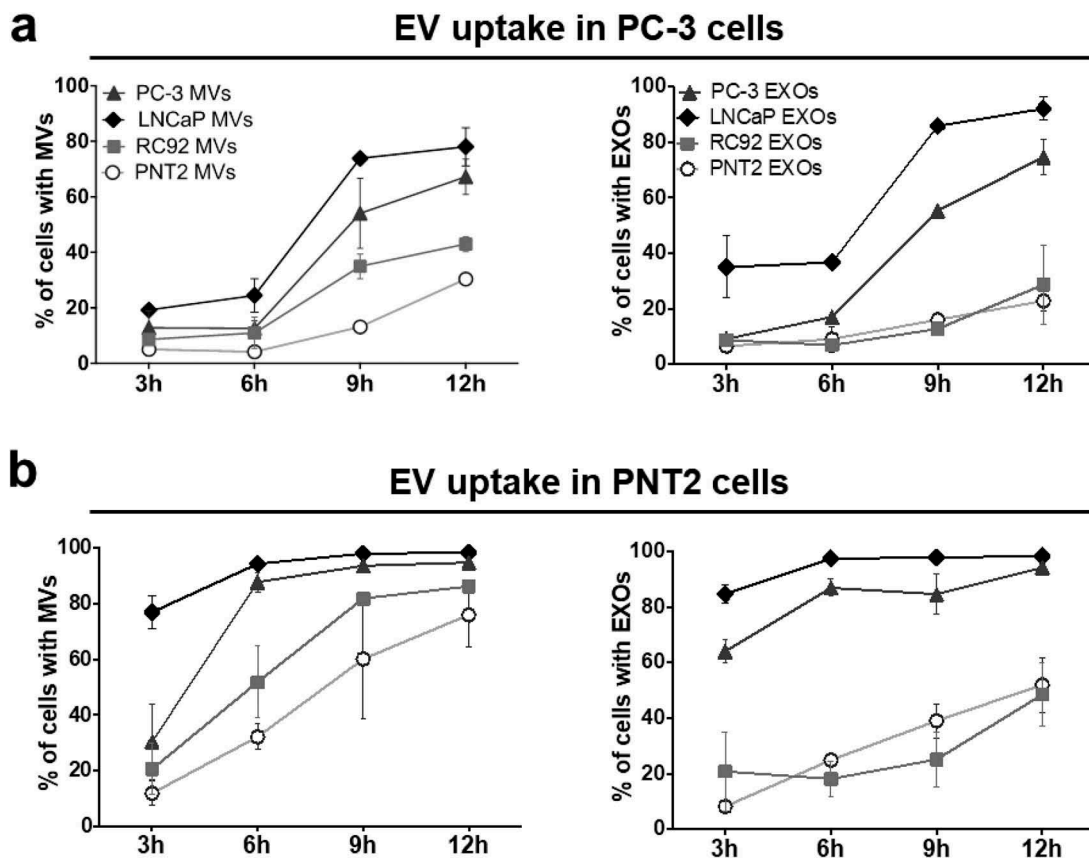


**Figure 3.** Uptake of prostate cell-derived 20K microvesicles and 110K exosomes analysed by high content microscopy. Fluorescently labelled 20K microvesicles (MVs) and 110K exosomes (EXOs) ( $10^9$  particles  $\text{ml}^{-1}$ ) from PC-3, LNCaP, RC92a/hTERT, and PNT2 cells were incubated with (a) PC-3 and (b) PNT2 cells for 3, 6, 9, and 12 h. An algorithm that segmented cellular features based on size and fluorescent intensity was used to analyse all images. Parameters were kept constant between different samples. Results represent percentage of cells with EVs normalised by the total number of cells. Dots represent the mean  $\pm$  SEM of two independent experiments.

continuous uptake in PC-3 cells (Figure 4(a)). Roughly, 30% of the total detected DiIC<sub>18</sub> EV-label was localised in the early endosomes and lysosomes. Only ~5% of DiIC<sub>18</sub>-EVs remained at the plasma membrane at 16 h, indicating efficient internalisation of EVs. Approximately 10% of DiIC<sub>18</sub>-label co-localised with Golgi marker GM130, possibly representing a part of the EVs that were released from the endosomal compartment (Figure 4(b)). The only difference in the partitioning of the PNT2 and PC-3 EV-label among the cell organelles was the higher proportion of the PNT2 EV-label in the early endosomes compared to the PC-3 EV-label (17% vs. 10%;  $p < 0.05$ ).

#### EV uptake by prostate cancer cells is influenced by the phase of cell cycle

To study whether cell cycle phase [resting phase/Gap1 ( $G_0/G_1$ ), DNA synthesis (S), Gap2 ( $G_2$ ) and mitosis (M)] has an effect on the uptake of EVs, we incubated PC-3 cells with DiOC<sub>18</sub>-labelled LNCaP EVs. LNCaP

and PC-3 EVs were selected for this assay, since they had the highest uptake and the fastest kinetics both in PC-3 and PNT2 cells (Figure 3). There were no statistically significant differences in the EV uptake of cells in the different cell cycle phases during the first 6 h (Supplementary Figure 1A). However, when 20K MVs were separately analysed, significantly higher EV signal was observed already at 3 h in the cells at the  $G_2/M$  phase (49% increase compared to  $G_0/G_1$ ;  $p < 0.001$ ) than cells in the S phase (39% increase compared to  $G_0/G_1$ ;  $p < 0.05$ ) (Supplementary Figure 1B).

After 24 h and 48 h, the PC-3 cells in the  $G_2/M$  phase had acquired a significantly higher EV signal than the cells in other cell cycle phases, also when the total population of LNCaP EVs (20K MV and 110K EXO) was analysed (Figure 5(a), 5(b)). A similar result was obtained when PC-3 cells were incubated with labelled PC-3 EVs for 24 h and 48 h (Figure 5(c), (d)), suggesting that the cellular uptake of EVs is increased during the  $G_2/M$  phase. To address the



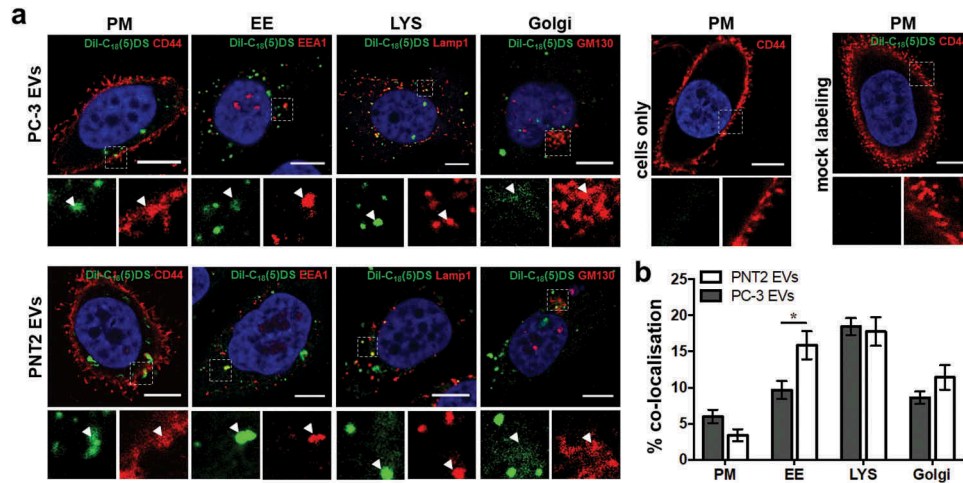


**Figure 4.** Localisation of the EV-associated DiI<sub>18</sub>(5)-DS label in prostate cells. (a) Cells were incubated for 16 h with PC-3 and PNT2 DiI<sub>18</sub>(5)-DS labelled EVs (DiI<sub>18</sub>-EVs) (pseudo-coloured green). Cells were immunostained with antibodies against CD44 for the localisation of plasma membrane (PM), EEA1 for early endosomes (EE), Lamp1 for lysosomes (LYS), and GM130 for Golgi (red), and imaged by confocal microscopy. Scale bars 10  $\mu$ m. Insets show a zoom into the organelle. (b) The percentage of the DiI<sub>18</sub> dye co-localisation with each antibody was quantified by Imaris software ( $n = 42$ –110 cells). Error bars represent the mean  $\pm$  SEM of 8–36 image frames each, \* $p < 0.05$  unpaired t-test.

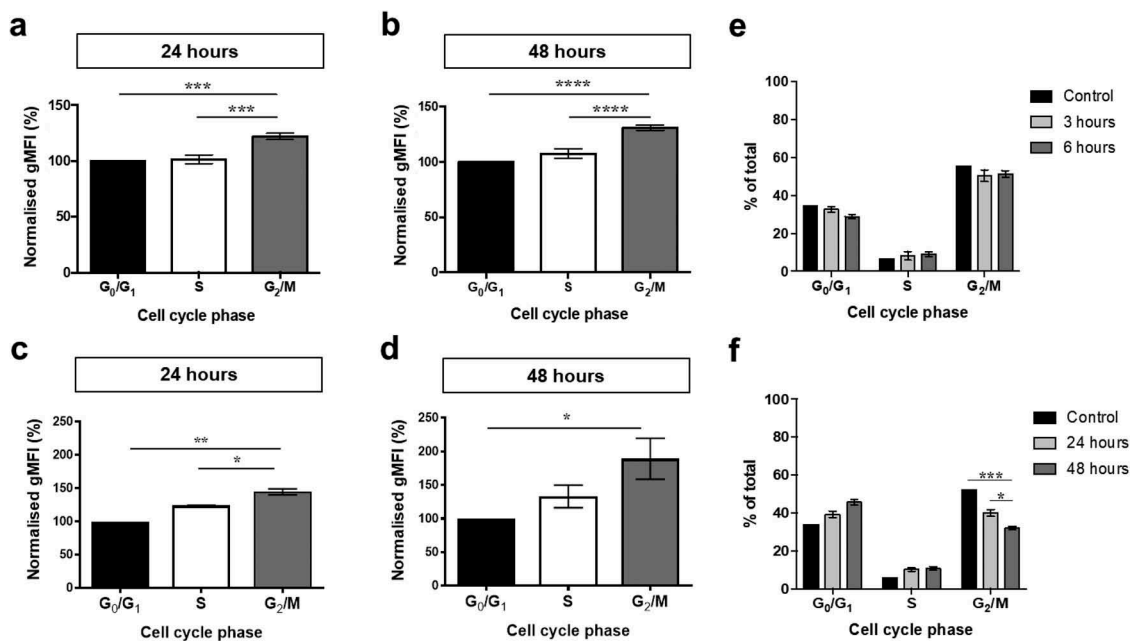


**Figure 5.** Uptake of prostate cell-derived EVs in the different stages of the cell cycle. PC-3 cells were incubated with SP-DiOC<sub>18</sub>-labelled LNCaP EVs for (a) 24 h or (b) 48 h, and SP-DiOC<sub>18</sub>-labelled PC-3 EVs for (c) 24 h or (d) 48 h. After fixation, the cells were stained with propidium iodide, and the SP-DiOC<sub>18</sub> fluorescence of cells was analysed by flow cytometry. The geometric mean fluorescence intensity (gMFI) of cells in each cell cycle phase was normalised by the fluorescence of cells in the G<sub>0</sub>/G<sub>1</sub> phase. Bars represent mean  $\pm$  SEM,  $n = 6$  per time point. \* $p < 0.05$ , \*\* $p < 0.01$ , \*\*\* $p < 0.001$ , \*\*\*\* $p < 0.0001$ , one-way ANOVA with Tukey's multiple comparisons test. Comparison of the percentage of cells incubated with and without (control) added EVs at the different phases of cell cycle at (e) 3 and 6 h, (f) 24 and 48 h. Error bars represent mean  $\pm$  SEM of six independent experiments. \* $p < 0.05$ , \*\*\* $p < 0.001$ , two-way ANOVA with Tukey's multiple comparisons test.

possibility that the EV uptake had stimulated the cells to enter the G<sub>2</sub>/M phase, we also analysed the distribution of cells in the different cell cycle phases during incubation with and without EVs. When cells were

incubated with EVs, the amount of cells in the G<sub>2</sub>/M phase of the cell cycle did not increase compared to the control cells, which were not incubated with EVs (Figure 5(e), 5(f)).

## Metastatic PCa EVs enhance proliferation and migration of prostate cells

The functional effects induced by the uptake of prostate cell-derived EVs were analysed by measuring proliferation and migration. Proliferation of PC-3 and PNT2 cells was analysed after 48 h and 72 h incubation with the EVs from the four different cell lines. At 48 h, no increase in cell proliferation was observed in the PC-3 cells incubated with any of the EVs (Figure 6(a)), while at 72 h, PC-3 cell proliferation was significantly increased in all EV-treated samples compared to the control without EVs (Figure 6(b)). EVs from the metastatic PC-3 cells enhanced proliferation more than twofold compared with the control, and significantly more than LNCaP, RC92a/hTERT and PNT2 EVs. In contrast to PC-3 cells, PNT2 cells showed increased proliferation already after 48 h incubation with the metastatic site-derived PC-3 and LNCaP EVs (Figure 6(c)). The biggest increase in the PNT2 cell proliferation at 48 and 72 h was observed in the cells incubated with PC-3 EVs, whose proliferation was twofold to fourfold compared with the control (Figure 6(c), 6(d)). Also, LNCaP EVs significantly enhanced PNT2 cell proliferation at 48 h, whereas no effect was observed with PNT2 and RC92 cell-derived EVs (Figure 6(c)).

Finally, the effect of the different prostate cell-derived EVs on PC-3 cell migration was investigated. Cell

migration was analysed until the gap closure was detected (at 6 h). Both metastatic and primary PCa-derived EVs (PC-3, LNCaP, and RC92a/hTERT) significantly stimulated migration of PC-3 cells (Figure 6(e), 6(f)), whereas the increase in migration by PNT2 EVs was not statistically significant from the control without EVs.

## Discussion

In this study, we compared EVs isolated from prostate cell lines with different PCa status: metastatic androgen-unresponsive PC-3, androgen-sensitive LNCaP, primary cancer cell-derived RC92a/hTERT, and the benign PNT2 prostate epithelial cells, to ask how the status of the parental cell line affects the uptake and the cancer-promoting effects of their EVs. Two different approaches, flow cytometry and fluorescent microscopy, were used to study uptake, which allowed less system-bias for the evaluation of EV uptake in general by analysing (a) the increase of EV-dependent fluorescence per cell and (b) the percentage of cells of the whole population, which were internalising EVs. Despite the apparent differences in the uptake kinetics at the early timepoints (Figure 3), the capacity of PC-3 prostate cancer and the benign PNT2 cells to internalise EVs was not statistically different between 3 and 9 h. As a summary, the properties of the PCa EVs rather than the

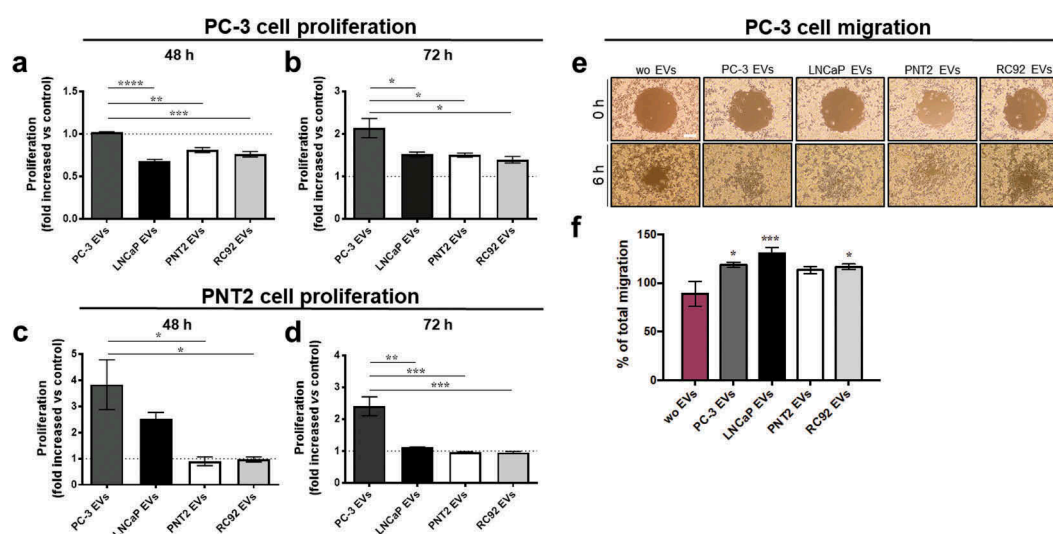


**Figure 6.** EVs from the metastatic PCa cells induce proliferation and migration in prostate cells. Cells were incubated with  $10^9$  EVs derived from PC-3, LNCaP, PNT2 and RC92a/hTERT cells or without (wo) EVs for the indicated times. The proliferation of (a,b) PC-3, and (c,d) the PNT2 cells, was measured using the CFSE-cellular staining by flow cytometry. The results are presented as the proliferation fold change compared to the control without EVs. Bars represent mean  $\pm$  SEM from three independent experiments. \* $p < 0.05$ , \*\* $p < 0.01$ , \*\*\* $p < 0.001$ , \*\*\*\* $p < 0.0001$ , one-way ANOVA with Tukey's multiple comparisons test. (e,f) Migration of PC-3 cells was monitored until gap closure at 6 h in cells incubated with PC-3, LNCaP, RC92a/hTERT, and PNT2-derived EVs or without EVs. Representative images show gap size at 0 and at 6 h (10 $\times$  magnification, scale bar 200  $\mu$ m). The percentage (%) of total migration of PC-3 cells after addition of EVs or in untreated control without EVs was calculated. Bars are mean  $\pm$  SEM from six independent experiments. \* $p < 0.05$ , \*\*\* $p < 0.001$ , one-way ANOVA with Dunnett's multiple comparisons test.

type of the recipient cells determined the efficiency and the kinetics of the uptake, so that the EVs derived from the cells of metastatic origin were more effectively internalised than those from benign or primary PCa cells. Our results are in line with those of Ronquist et al. [32] showing both faster kinetics for PC-3 EXOs compared to non-cancerous prostasomes, and a somewhat enhanced uptake to the benign CRL2221 prostate cells at early time points. Confirming our previous results with PC-3 and LNCaP cells [33], no differences in the trends of the uptake of the 20K MV and 110K EXO enriched subpopulations were observed.

More than the cancer vs. non-cancerous status of the recipient cells, the phase in the cell cycle affected the EV uptake. EV internalisation during the G<sub>2</sub>/M phase was enhanced in comparison to the G<sub>0</sub>/G<sub>1</sub> and S phases. Although our data cannot fully exclude the possibility that the higher EV signal in the mitotic cells was due to the stimulation of mitosis by EVs, we did not observe any increase in the proportion of cells in the G<sub>2</sub>/M phase, when the cells incubated with EVs were compared to the control without EVs. Supporting our finding, the internalisation of artificial nanoparticles was also reported to be most efficient at the G<sub>2</sub>/M phase [34]. This is to our knowledge the first observation of the effect of the cell cycle on EV uptake. Enhanced EV uptake by actively dividing cancer cells could be a way to further stimulate cancer cell growth, as EVs in general have been shown to promote cell proliferation [35–38].

Several mechanisms for cellular uptake of EVs have been postulated [39], including energy-dependent receptor-mediated endocytosis (clathrin-mediated and caveolin-mediated) [40,41], micropinocytosis [41,42], phagocytosis [31,43], and plasma membrane or endosomal-mediated fusion [44,45]. In our experiments, roughly 30% of the fluorescent EV label was co-localised with the endo-lysosomal compartment, which is in line with the concept that EVs are taken up through endocytosis [40,41], although the possibility of the EV fusion at the plasma membrane could not be excluded.

Strikingly, metastatic site-derived EVs were most efficiently internalised by both prostate cancer and benign cells. We speculate that the faster internalisation and intracellular trafficking of metastatic cancer cell-derived EVs could depend on, for example, their surface protein composition [46]. In line with this hypothesis, trypsinisation of the outer surface proteins from 20K MVs decreased their uptake in PC-3 cells, when indirectly measured as EV-delivered paclitaxel cytotoxicity [33]. Recently, also an ATP-usage dependent differential uptake of prostasomes and PC-3 cell-derived EXOs by normal and prostate cancer cells was described, which may offer a mechanism for the differential uptake [32].

The higher co-localisation of the PNT2 EVs with the early endosomes compared to the PC-3 EVs could reflect a slower uptake of the non-cancerous EVs, or for example, different intracellular trafficking. Since the lipophilic dyes cannot be used to follow the EV cargo after cell entry, future studies with a combined labelling of EV lipids and nucleic acids or proteins are needed for a better insight of the EV trafficking inside the cell.

Finally, supplementing previous findings [46,47], our data showing that the metastatic cell-derived EVs enhanced proliferation and cell migration of cancer and non-cancerous cells supports the concept that the metastatic EVs promote tumour-benefiting functions. In this respect, the finding that the benign cells rapidly and efficiently internalised the metastatic EVs may be of significance. Our results also support the earlier findings of an active role of EVs in PCa progression [48] and warrant further broad “omics” approaches to reveal the EV-borne molecular machinery responsible for these effects. We and others have previously shown that the genomic [24], transcriptomic [25], proteomic [49,50], metabolomics [51] and lipidomic [52] profiles of PCa EVs are variable and dependent on the cancerous status of the parent cell. Suggested by our study, broader cell-line based comparisons may help to dissect the molecular differences modifying the behaviour of prostate cells in the tumour and/or metastatic environment. Considering the already known importance of the EV-mediated communication in the PCa tumour progression [53,54], it will be relevant to systematically compare EVs of different origins and to analyse their cargo to unravel the EV-based communication mechanisms between cancerous and non-cancerous cells.

## Acknowledgements

The authors acknowledge Patricia Ramos Ramírez for her kind assistance with the proliferation experiments, and the Extracellular Vesicle Core Facility, University of Helsinki for the EV analytics.

## Disclosure statement

No potential conflict of interest was reported by the authors.

## Funding


This work was supported by the Academy of Finland [grants © 287089 (MN, PS), ©259990 (MY)], Orion Foundation (MY), The Medicinska Understödsföreningen Liv och Hälsa r.f. (PS), Otto Malm Foundation (PS), and Magnus Ehrnrooth Foundation (MT, PS). Part of the study was supported by the Salve Research Programme for GET IT DONE (Tekes- the Finnish Funding Agency for Technology and Innovation) [grant © 534/14 and 3986/31/2013 ©] (ELI, MT, MY, PS).

## Geolocation

University of Helsinki, Finland (60.1695, 24.9354)

## ORCID


Elisa Lázaro-Ibáñez  <http://orcid.org/0000-0002-3542-7069>

Maarit Neuvonen  <http://orcid.org/0000-0002-7209-3029>

Maarit Takatalo  <http://orcid.org/0000-0003-4825-6358>

Vincenzo Cerullo  <http://orcid.org/0000-0003-4901-3796>

Kirsi Rilla  <http://orcid.org/0000-0002-7862-5727>

Pia R.-M. Siljander  <http://orcid.org/0000-0003-2326-5821>

## References

- [1] Mittelbrunn M, Sánchez-Madrid F. Intercellular communication: diverse structures for exchange of genetic information. *Nat Rev Mol Cell Biol.* **2012**;13(5):328–335.
- [2] Yáñez-Mó M, Siljander PR, Andreu Z, et al. Biological properties of extracellular vesicles and their physiological functions. *J Extracell Vesicles.* **2015**;4.
- [3] Théry C, Ostrowski M, Segura E. Membrane vesicles as conveyors of immune responses. *Nat Rev Immunol.* **2009**;9(8):581–593.
- [4] Colombo M, Raposo G, Théry C. Biogenesis, secretion, and intercellular interactions of exosomes and other extracellular vesicles. *Annu Rev Cell Dev Biol.* **2014**;30:255–289.
- [5] Valadi H, Ekström K, Bossios A, et al. Exosome-mediated transfer of mRNAs and microRNAs is a novel mechanism of genetic exchange between cells. *Nat Cell Biol.* **2007**;9(6):654–659.
- [6] Ratajczak J, Wysoczynski M, Hayek F, et al. Membrane-derived microvesicles: important and underappreciated mediators of cell-to-cell communication. *Leukemia.* **2006**;20(9):1487–1495.
- [7] Deregibus MC, Cantaluppi V, Calogero R, et al. Endothelial progenitor cell derived microvesicles activate an angiogenic program in endothelial cells by a horizontal transfer of mRNA. *Blood.* **2007**;110(7):2440–2448.
- [8] Barry OP, Pratico D, Lawson JA, et al. Transcellular activation of platelets and endothelial cells by bioactive lipids in platelet microparticles. *J Clin Invest.* **1997**;99(9):2118–2127.
- [9] Zhao H, Yang L, Baddour J, et al. Tumor microenvironment derived exosomes pleiotropically modulate cancer cell metabolism. *Elife.* **2016**;5:e10250.
- [10] Skog J, Würdinger T, Van Rijn S, et al. Glioblastoma microvesicles transport RNA and proteins that promote tumour growth and provide diagnostic biomarkers. *Nat Cell Biol.* **2008**;10(12):1470–1476.
- [11] Costa-Silva B, Aiello NM, Ocean AJ, et al. Pancreatic cancer exosomes initiate pre-metastatic niche formation in the liver. *Nat Cell Biol.* **2015**;17(6):816–826.
- [12] Peinado H, Alečković M, Lavotshkin S, et al. Melanoma exosomes educate bone marrow progenitor cells toward a pro-metastatic phenotype through MET. *Nat Med.* **2012**;18(6):883–891.
- [13] Al-Nedawi K, Meehan B, Micallef J, et al. Intercellular transfer of the oncogenic receptor EGFRvIII by microvesicles derived from tumour cells. *Nat Cell Biol.* **2008**;10(5):619–624.
- [14] Hoshino A, Costa-Silva B, Shen T, et al. Tumour exosome integrins determine organotropic metastasis. *Nature.* **2015**;527(7578):329–335.
- [15] Renzulli JF, Del Tatto M, Dooner G, et al. Microvesicle induction of prostate specific gene expression in normal human bone marrow cells. *J Urol.* **2010**;184(5):2165–2171.
- [16] Panagopoulos K, Cross-Knorr S, Dillard C, et al. Reversal of chemosensitivity and induction of cell malignancy of a non-malignant prostate cancer cell line upon extracellular vesicle exposure. *Mol Cancer.* **2013**;12(1):118.
- [17] Fedele C, Singh A, Zerlanko BJ, et al. The alphavbeta6 integrin is transferred intercellularly via exosomes. *J Biol Chem.* **2015**;290(8):4545–4551.
- [18] Hosseini-Beheshti E, Choi W, Weiswald LB, et al. Exosomes confer pro-survival signals to alter the phenotype of prostate cells in their surrounding environment. *Oncotarget.* **2016**;7(12):14639–14658.
- [19] Castellana D, Zobairi F, Martinez MC, et al. Membrane microvesicles as actors in the establishment of a favorable prostatic tumoral niche: a role for activated fibroblasts and CX3CL1-CX3CR1 axis. *Cancer Res.* **2009**;69(3):785–793.
- [20] Itoh T, Ito Y, Ohtsuki Y, et al. Microvesicles released from hormone-refractory prostate cancer cells facilitate mouse pre-osteoblast differentiation. *J of Mol Histol.* **2012**;43(5):509–515.
- [21] Huang X, Yuan T, Liang M, et al. Exosomal miR-1290 and miR-375 as prognostic markers in castration-resistant prostate cancer. *Eur Urol.* **2015**;67(1):33–41.
- [22] Overbye A, Skotland T, Koehler CJ, et al. Identification of prostate cancer biomarkers in urinary exosomes. *Oncotarget.* **2015**;6(30):30357–30376.
- [23] Wang L, Skotland T, Berge V, et al. Exosomal proteins as prostate cancer biomarkers in urine: from mass spectrometry discovery to immunoassay-based validation. *Eur J Pharm Sci.* **2017**;98(Feb 15):80–85.
- [24] Lázaro-Ibáñez E, Sanz-García A, Visakorpi T, et al. Different gDNA content in the subpopulations of prostate cancer extracellular vesicles: apoptotic bodies, microvesicles, and exosomes. *Prostate.* **2014**;74(14):1379–1390.
- [25] Lázaro-Ibáñez E, Lunavat TR, Jang SC, et al. Distinct prostate cancer-related mRNA cargo in extracellular vesicle subsets from prostate cell lines. *BMC Cancer.* **2017**;17(1):92.
- [26] Royo F, Zuniga-Garcia P, Torrano V, et al. Transcriptomic profiling of urine extracellular vesicles reveals alterations of CDH3 in prostate cancer. *Oncotarget.* **2016**;7(6):6835–6846.
- [27] McKiernan J, Donovan MJ, O'Neill V, et al. A novel urine exosome gene expression assay to predict high-grade prostate cancer at initial biopsy. *JAMA Oncol.* **2016**;2(7):882–889.
- [28] Gu Y, Li H, Miki J, et al. Phenotypic characterization of telomerase-immortalized primary non-malignant and malignant tumor-derived human prostate epithelial cell lines. *Exp Cell Res.* **2006**;312(6):831–843.
- [29] Morelli AE, Larregina AT, Shufesky WJ, et al. Endocytosis, intracellular sorting, and processing of exosomes by dendritic cells. *Blood.* **2004**;104(10):3257–3266.

- [30] Escrevente C, Keller S, Altevogt P, et al. Interaction and uptake of exosomes by ovarian cancer cells. *BMC Cancer*. 2011;11(1):1.
- [31] Christianson HC, Svensson KJ, Van Kuppevelt TH, et al. Cancer cell exosomes depend on cell-surface heparan sulfate proteoglycans for their internalization and functional activity. *Proc Natl Acad Sci U S A*. 2013;110(43):17380–17385.
- [32] Ronquist KG, Sanchez C, Dubois L, et al. Energy-requiring uptake of prostasomes and PC3 cell-derived exosomes into non-malignant and malignant cells. *J Extracell Vesicles*. 2016;5:29877.
- [33] Saari H, Lázaro-Ibáñez E, Viitala T, et al. Microvesicle and exosome-mediated drug delivery enhances the cytotoxicity of Paclitaxel in autologous prostate cancer cells. *J Controlled Release*. 2015 Dec 28;220, Part B:727–737.
- [34] Kim JA, Åberg C, Salvati A, et al. Role of cell cycle on the cellular uptake and dilution of nanoparticles in a cell population. *Nat Nanotech*. 2012;7(1):62–68.
- [35] O'Brien K, Rani S, Corcoran C, et al. Exosomes from triple-negative breast cancer cells can transfer phenotypic traits representing their cells of origin to secondary cells. *Eur J Cancer*. 2013;49(8):1845–1859.
- [36] Yang L, Wu X, Wang D, et al. Bladder cancer cell-derived exosomes inhibit tumor cell apoptosis and induce cell proliferation in vitro. *Mol Med Rep*. 2013;8(4):1272–1278.
- [37] Lindoso RS, Collino F, Camussi G. Extracellular vesicles derived from renal cancer stem cells induce a protumorigenic phenotype in mesenchymal stromal cells. *Oncotarget*. 2015;6(10):7959–7969.
- [38] Haga H, Yan IK, Takahashi K, et al. Tumour cell-derived extracellular vesicles interact with mesenchymal stem cells to modulate the microenvironment and enhance cholangiocarcinoma growth. *J Extracell Vesicles*. 2015;4:24900.
- [39] Mulcahy LA, Pink RC, Carter DRF. Routes and mechanisms of extracellular vesicle uptake. *J Extracell Vesicles*. 2014;3:24641.
- [40] Svensson KJ, Christianson HC, Wittrup A, et al. Exosome uptake depends on ERK1/2-heat shock protein 27 signaling and lipid Raft-mediated endocytosis negatively regulated by caveolin-1. *J Biol Chem*. 2013;288(24):17713–17724.
- [41] Tian T, Zhu Y, Hu F, et al. Dynamics of exosome internalization and trafficking. *J Cell Physiol*. 2013;228(7):1487–1495.
- [42] Fitzner D, Schnaars M, Van Rossum D, et al. Selective transfer of exosomes from oligodendrocytes to microglia by macropinocytosis. *J Cell Sci*. 2011;124(Pt 3):447–458.
- [43] Feng D, Zhao W, Ye Y, et al. Cellular internalization of exosomes occurs through phagocytosis. *Traffic*. 2010;11(5):675–687.
- [44] Del Conde I, Shrimpton CN, Thiagarajan P, et al. Tissue-factor-bearing microvesicles arise from lipid rafts and fuse with activated platelets to initiate coagulation. *Blood*. 2005;106(5):1604–1611.
- [45] Parolini I, Federici C, Raggi C, et al. Microenvironmental pH is a key factor for exosome traffic in tumor cells. *J Biol Chem*. 2009;284(49):34211–34222.
- [46] Harris DA, Patel SH, Gucek M, et al. Exosomes released from breast cancer carcinomas stimulate cell movement. *PloS One*. 2015;10(3):e0117495.
- [47] Whitehead B, Wu L, Hvam ML, et al. Tumour exosomes display differential mechanical and complement activation properties dependent on malignant state: implications in endothelial leakiness. *J Extracell Vesicles*. 2015;4:29685.
- [48] Liu C, Hsieh C, Shen C, et al. Exosomes from the tumor microenvironment as reciprocal regulators that enhance prostate cancer progression. *International J Urol*. 2016;23(9):734–744.
- [49] Duijvesz D, Burnum-Johnson KE, Gritsenko MA, et al. Proteomic profiling of exosomes leads to the identification of novel biomarkers for prostate cancer. *PloS One*. 2013;8(12):e82589.
- [50] Jansen FH, Krijgsveld J, Van Rijswijk A, et al. Exosomal secretion of cytoplasmic prostate cancer xenograft-derived proteins. *Mol Cell Proteomics*. 2009;8(6):1192–1205.
- [51] Puhka M, Takatalo M, Nordberg M, et al. Metabolomic profiling of extracellular vesicles and alternative normalization methods reveal enriched metabolites and strategies to study prostate cancer -related changes. *Theranostics*. Forthcoming 2017.
- [52] Llorente A, Skotland T, Sylvänne T, et al. Molecular lipidomics of exosomes released by PC-3 prostate cancer cells. *BBA Mol Cell Biol Lipids*. 2013;1831(7):1302–1309.
- [53] Ramteke A, Ting H, Agarwal C, et al. Exosomes secreted under hypoxia enhance invasiveness and stemness of prostate cancer cells by targeting adherens junction molecules. *Mol Carcinog*. 2015;54(7):554–565.
- [54] Abd Elmageed ZY, Yang Y, Thomas R, et al. Neoplastic reprogramming of patient-derived adipose stem cells by prostate cancer cell-associated exosomes. *Stem Cells*. 2014;32(4):983–997.